

Dynamic Modelling and Acceleration Signal Analysis of Rail Surface Defects for Enhanced Rail Condition Monitoring and Diagnosis

Andrew Keong Ng*, Landong Martua
 Singapore Institute of Technology
 Singapore
 e-mail: Andrew.Ng@SingaporeTech.edu.sg

George Sun
 Land Transport Authority
 Singapore

Abstract—Early detection of rail surface defects (RSDs) is crucial for timely rail maintenance, repair, or replacement to prevent potential risk of rail breaks and train derailments. Axle box acceleration (ABA) measurement is commonly used to identify rail and track irregularities. This paper aims to (1) model and simulate three common RSDs (rail corrugation, spalling, and squat) with three severity levels (light, moderate, and severe); (2) process and analyse simulated RSD-driven ABA signals; and (3) ascertain relationships between RSDs and their corresponding ABA signals. Explicit dynamic finite element models of wheel-rail interaction were created for rails with and without RSDs. Simulated RSD-driven ABA signals were subsequently processed and analysed using various signal processing algorithms including short-time Fourier transform, continuous wavelet transform, empirical mode decomposition, and power spectral density. Results reveal the likelihood of automatically detecting and classifying different types and different severity levels of RSDs from ABA signals, thereby enhancing the efficiency and effectiveness of rail condition monitoring and diagnosis.

Keywords- rail surface defects; wheel-rail interaction; modelling and simulation; axle-box acceleration; signal processing and analysis; condition monitoring and diagnosis

I. INTRODUCTION

Rail is a key component of a railway track; it supports and guides the trains that carry people, animals, and goods from one place to another. As the contact area between wheel and rail is small, rail surface is constantly subjected to high contact pressure. Rail surface defects (RSDs) are consequently developed due to fluctuation of wheel-rail contact pressure, rolling contact fatigue, as well as rail bending, thermal, and residual stresses [1]. RSDs elevate wheel-rail contact pressure and augment vehicle-track vibration and noise level, creating an unsafe and unpleasant commute. According to their appearances, RSDs can be broadly categorised into two groups: rail corrugation and rail contact fatigue defects [1]. Rail corrugation has a quasi-periodic wear pattern, whereas rail contact fatigue defects, for instance, flaking, spalling, squats, and shelling, have no repeating patterns.

To avoid potential risk associated with rail breaks and train derailments, early detection of RSDs is of vital importance so that rail maintenance, repair, or replacement can be performed in a timely manner. Rail surface is routinely inspected by track maintenance staff during non-revenue hours, which can be labour-intensive, time-

consuming, subjective, and weather-dependent. Furthermore, RSDs may grow and worsen between track inspection intervals, threatening the reliability and safety of railway operation. To address the shortcomings of human visual inspection, track inspection trolleys and multi-function vehicles are deployed [2]. Piezo-accelerometers or fiber laser accelerometers are usually mounted on axle box or bogie to identify rail and track irregularities [3-5] because axle box acceleration (ABA) measurement is inexpensive, easy to install and maintain, and efficacious.

For enhanced rail condition monitoring and diagnosis, it is indispensable to appropriately recognise different types and different severity levels of RSDs from ABA signals. However, there is limited information regarding RSDs and their corresponding ABA signals. This paper, therefore, aims to (1) model and simulate three common RSDs (rail corrugation, spalling, and squat) with three severity levels (light, moderate, and severe); (2) process and analyse simulated RSD-driven ABA signals; and (3) ascertain relationships between RSDs and their corresponding ABA signals.

II. MODELLING AND SIMULATION OF SMOOTH RAIL

An explicit dynamic finite element (FE) model of wheel-rail interaction was carefully created using Abaqus software package because geometry and input parameters can influence vehicle-track dynamic and contact solutions [6]. Geometry of wheels, rails, and sleepers were obtained from precise engineering drawings. The rail is UIC60 type, with a length of 24 m to avoid wave reflection from both rail ends. Symmetric assumption was made in the FE model because vehicle was assumed running on straight track with insignificant wheel lateral motion [5]. Thus, only half vehicle-track system was constructed. Fig. 1a presents the schematic diagram and nomenclature in FE model of wheel-rail interaction. Other railway track components, such as primary suspension, fasteners, and ballasts, were modelled as springs and dampers with stiffness and damping values listed in Table I.

Wheel, rail, and sleepers were meshed using three-dimensional, eight-node linear hexahedral elements with reduced integration and hourglass control. Element sizes were controlled to obtain highly precise solution, while maintaining reasonable computation time. In stabilization and solution zones of wheel-rail contact, where precise contact pressure distributions are desirable, we utilised an

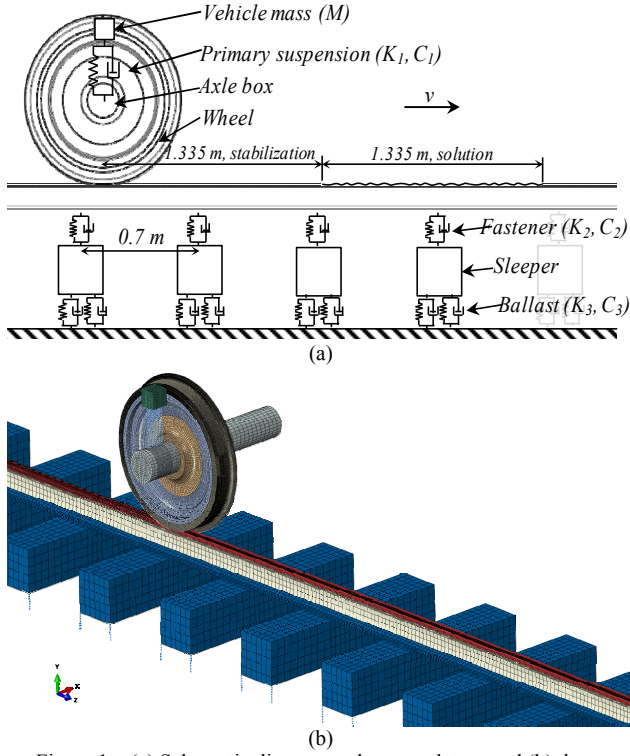


Figure 1. (a) Schematic diagram and nomenclature and (b) three-dimensional FE model of wheel-rail interaction.

element size of 1.3 mm, as depicted in Fig. 1b. Surface-to-surface penalty contact algorithm with static and dynamic friction coefficient of 0.3 was also considered in the wheel-rail contact model.

Similar to our earlier approaches [7-9], a vehicle-track implicit static equilibrium analysis was performed to close the gap between wheel and rail, as well as to obtain structure deformation caused by gravitational load. This step was deemed as initial conditions for vehicle-track explicit dynamic analysis. Moreover, a 1.335 m of rolling distance from initial wheel position to the solution zone was included in the FE model to stabilise initial vibration resulted from transition of implicit to explicit solution. This rolling distance is equivalent to a half of the wheel rotation. Simulated ABA signals were extracted from the element set representing axle box.

III. MODELLING AND SIMULATION OF RSDs

A. Rail Corrugation

Rail corrugation is a quasi-periodic undulatory wear on the rail top surface [1]. Under light nominal axle load passenger operations, short-pitch corrugation with a wear depth of below 0.2-0.3 mm is typically found. Rail corrugation was modelled in accordance with the rail wear profile prediction model in [7], which is an iterative process encapsulating local wheel-rail contact analysis, rail wear estimation, as well as rail surface geometry update and

TABLE I. MODEL PARAMETERS AND MATERIAL PROPERTIES

Component	Parameter	Value
<u>Wheel, axle, and rail parameters</u>		
Wheel, axle, and rail	Young's modulus	203 GPa
	Poisson's ratio	0.3
	Density	7800 kg/m ³
	Yield stress	800 MPa
	Tangent modulus	21 GPa
<u>Vehicle parameters</u>		
Sprung mass	Mass, M	10000 kg
	Velocity, v	50.4 km/h
Primary suspension	Stiffness, K_1	1.15 MN/m
	Damping, C_1	2500 kNs/m
<u>Track parameters</u>		
Fastener	Stiffness, K_2	1300 MN/m
	Damping, C_2	45 kNs/m
Sleeper	Young's modulus	20.3 GPa
	Poisson's ratio	0.21
	Density	115.7 kg/m ³
Ballast	Stiffness, K_3	45 MN/m
	Damping, C_3	32 kNs/m

smoothing. Archard's wear law was adopted to predict the removal of rail surface material in the lateral and longitudinal directions. Fig. 2 displays the rail corrugation profiles with average wear depths of 0.02 mm and 0.2 mm.

B. Spalling

Unlike rail corrugation, spalling is a surface-initiated rail contact fatigue defect [1]. It is originated from head checks at the gauge corner surface. When several head checks propagate and intersect, small chip of rail material spalls out and over time grows into moderate and severe spalling. Fig 3 illustrates the spalling profiles in [1], where the depths for light, moderate, and severe spalling are 0.05 mm, 0.10 mm, and 0.2 mm, respectively.

C. Squat

A squat is originated from either small cracks at white etching layer on the rail top surface or checks on gauge corner [1]. There are three classes of squats [10]: light squat (length = 15 mm, depth = 0.05 mm), moderate squat (length = 37 mm, depth = 0.10 mm), and severe squat (length = 61 mm, depth = 0.2 mm). Fig. 4 plots the longitudinal profiles of these three squats, which have visual accompanying V, U, Y or circular shaped cracks that resemble a very heavy gnome has sat or squat on the rail.

IV. ANALYSIS OF RSD-DRIVEN ABA SIGNALS

Simulated ABA signals for the three common RSDs (rail corrugation, spalling, and squat) with three severity levels

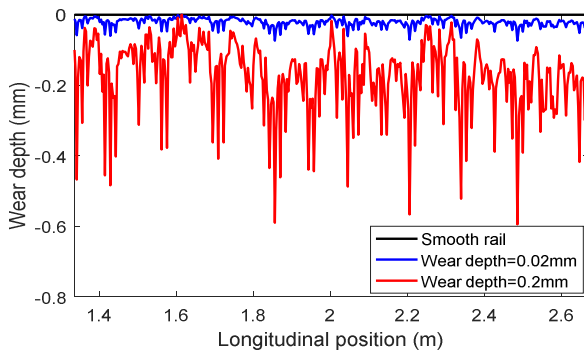


Figure 2. Rail corrugation profiles for smooth rail and corrugated rails with average wear depth of 0.02 mm and 0.20 mm.

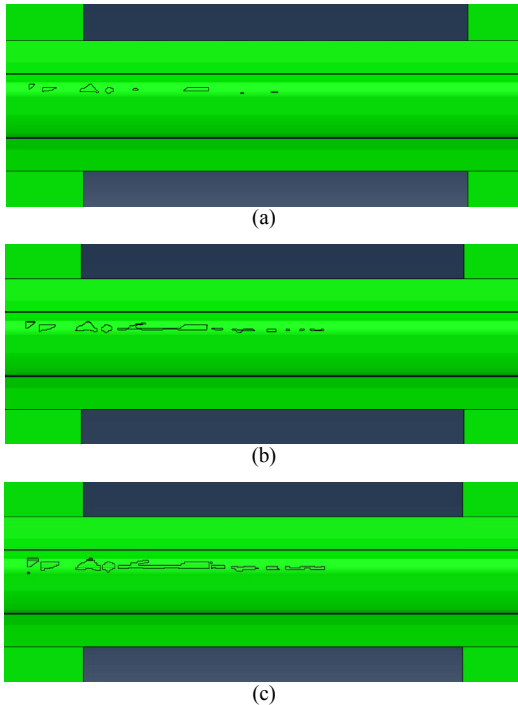


Figure 3. Profiles in FE model for (a) light, (b) moderate, and (c) severe spalling.

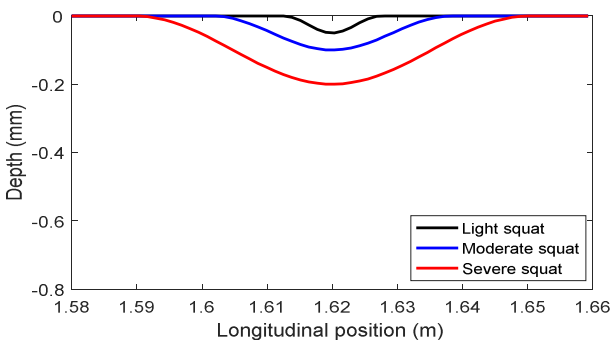


Figure 4. Profiles in FE model for (a) light, (b) moderate, and (c) severe squats.

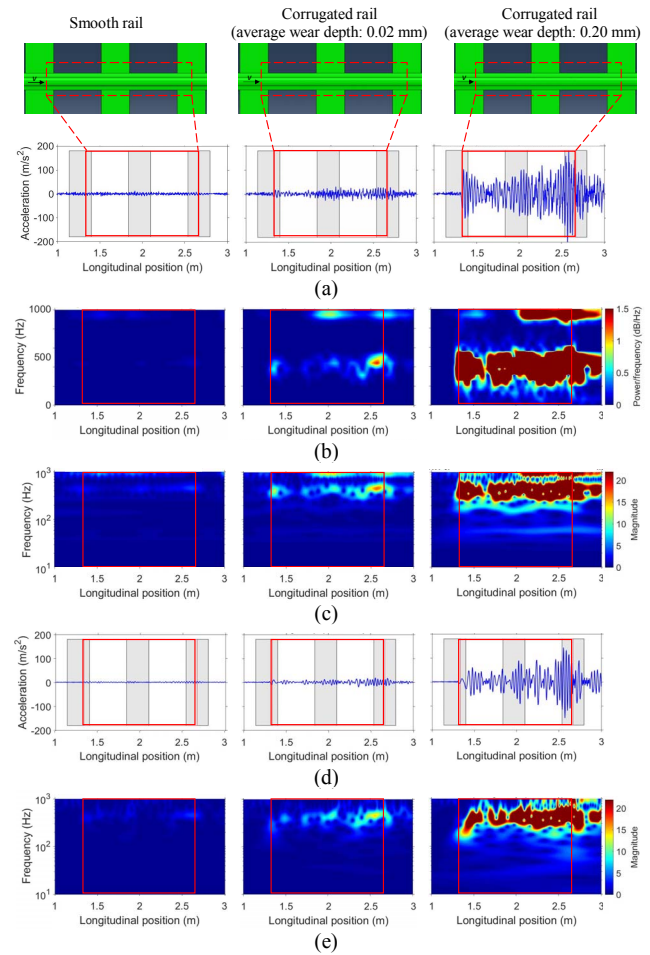


Figure 5. Signal analysis for smooth and corrugated rails: (a) simulated signals, (b) STFT, (c) CWT, (d) IMF2, and (e) CWT of IMF2.

(light, moderate, and severe) were processed and analysed using a variety of signal processing algorithms within Matlab software package; these algorithms involve short-time Fourier transform (STFT) [4], continuous wavelet transform (CWT) [10], empirical mode decomposition (EMD) [11], and power spectral density (PSD).

Fig. 5a shows the ABA signals for smooth rail and corrugated rails with average wear depth of 0.02 mm and 0.2 mm. It is apparent that ABA signals for smooth rail has the smallest amplitude, and the signal amplitude increases with corrugation severity. A similar observation is made for spalling and squat, as shown in Fig. 6a and Fig. 7a, respectively.

Owing to the fact that temporal features of ABA signals are inadequate to accurately detect and classify dissimilar RSDs, spectral and spectral-temporal features of ABA signals were also examined in this paper. Fig. 5b, Fig. 6b, and Fig. 7b renders the STFT of ABA signals driven by rail corrugation, spalling, and squat. The signals, whose sampling frequency is 4000 Hz, were analysed using Hann window of length 64 samples and 75% overlap. While the spectral characteristics of RSDs are exhibited in their respective spectrograms, there is a compromise between time

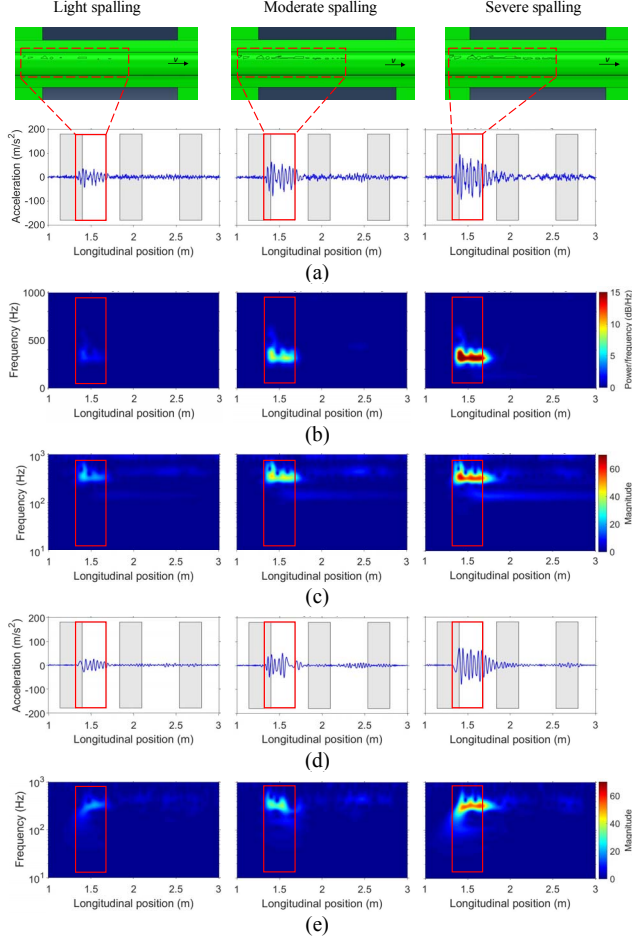


Figure 6. Signal analysis for light, moderate, and severe spalling: (a) simulated signals, (b) STFT, (c) CWT, (d) IMF2, and (e) CWT of IMF2.

and frequency resolution. A narrow-width window generates a good resolution in time domain, but yields a poor resolution in frequency domain, and vice versa, which may not be suitable for analysing different RSDs with varying severities.

CWT was employed in order to achieve optimal time and frequency resolutions at dissimilar frequency bands. RSD-driven ABA signals were multiplied by a group of shifted and scaled versions of Morlet wavelet function. The CWT plots of rail corrugation, spalling, and squat are respectively presented in Fig. 5c, Fig. 6c, and Fig. 7c.

To better comprehend the spectral-temporal characteristics of RSDs, we propose the integration of EMD and CWT. EMD is self-adaptive to diverse signals and can handle nonstationary and nonlinear signals [11], just like those induced by rail corrugation, spalling, and squat. The RSD-driven signals were first decomposed into a series of intrinsic mode functions (IMFs) representing fast to slow oscillations in the signals. Each IMF signifies a simple oscillatory mode with variable amplitude and frequency as functions of time, instead of a simple harmonic function with constant amplitude and frequency; hence, it can improve the physical meaning of instantaneous amplitude and

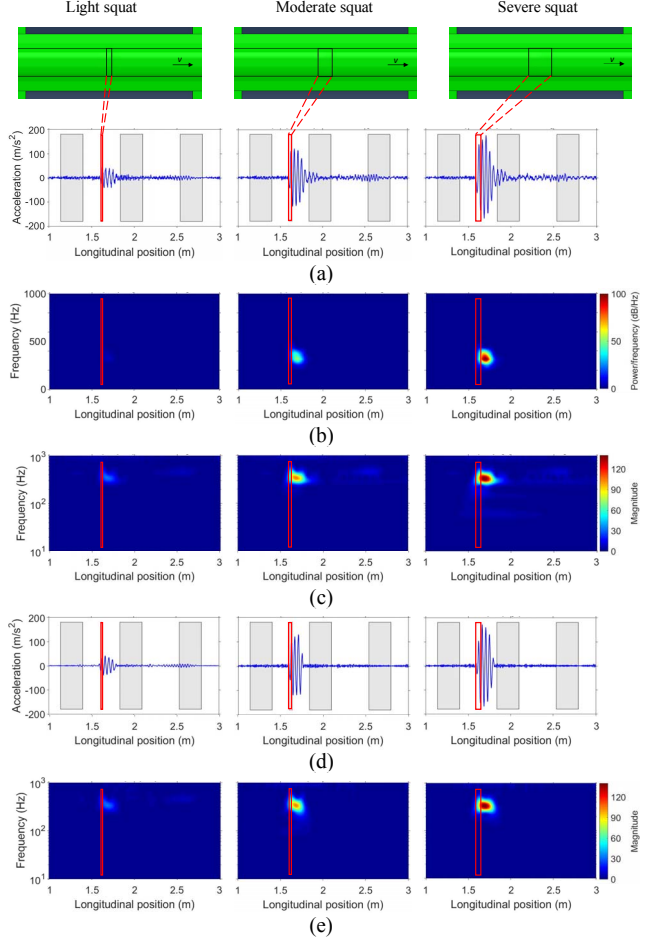


Figure 7. Signal analysis for light, moderate, and severe squats: (a) simulated signals, (b) STFT, (c) CWT, (d) IMF2, and (e) CWT of IMF2.

instantaneous frequencies. Fig. 5d, Fig. 6d, and Fig. 7d depicts the second IMF (IMF2), which contains the most natural frequencies of the RSDs. Subsequently, CWT was applied to the IMF2, as illustrated in Fig. 5e, Fig. 6e, and Fig. 7e for rail corrugation, spalling, and squat, respectively. It can be observed that random noise embedded in the ABA signals has been effectively reduced while preserving signal energy.

In addition, we noticed that the dominant frequency of rail corrugation ranges from 239 Hz to 675 Hz. High signal energy occurs at the corrugation location and remains somewhat high even after that. This implies that the vehicle and track experience free vibration after been excited by corrugation, and the vibration gradually decays after the vehicle has passed the corrugation location. On the contrary, the dominant frequency of spalling ranges between 194 Hz and 630 Hz. High signal energy occurs at the spalling location of spalling. In contrast, the dominant frequency of squat ranges from 111 Hz to 446 Hz. Unlike rail corrugation and spalling, higher signal energy are noted when the wheel passes over the squat, but not when it touches the squat. This phenomenon is known as de-stressing and re-stressing phases [12] and agrees with the finding in [5].

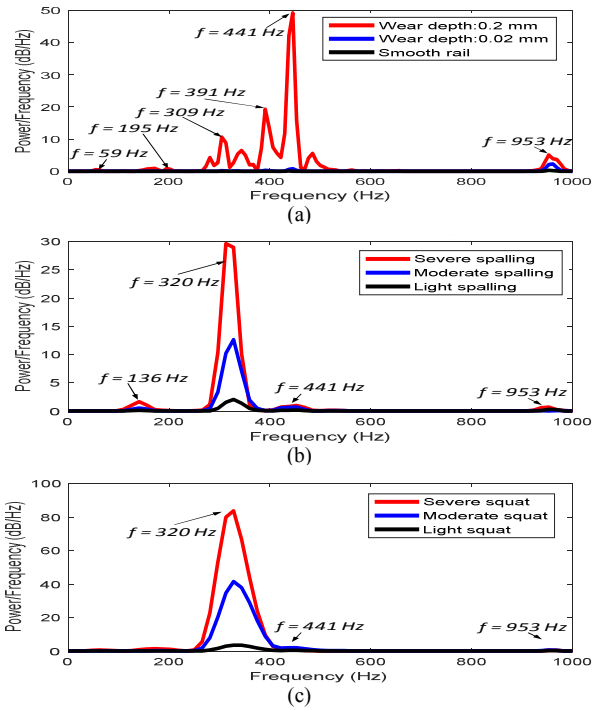


Figure 8. PSD of RSD-driven ABA signals for different severity levels:
(a) rail corrugation, (b) spalling, and (c) squat.

PSD of RSD-driven ABA signals were also evaluated and plotted in Fig. 8. For all the RSDs, signal powers consistently increase with severity levels, implying greater intensity of vibrations for higher severities. For smooth rail, the peak magnitude and frequency are respectively 0.4 dB at 953 Hz. For corrugated rails with average wear depths of 0.02 mm and 0.2 mm, the peak magnitude and frequency are respectively 2.3 dB at 953 Hz and 49 dB at 441 Hz, which corresponds to a short-pitch corrugation. For light, moderate, and severe spalling, the peak frequency is at 320 Hz, but the power magnitudes are respectively 2 dB, 13 dB, and 30 dB. Relative to spalling, squats possess shorter duration and higher power magnitudes of 3.5 dB, 41 dB, and 84 dB at peak frequency of 320 Hz for light, moderate, and severe squats, respectively.

V. DISCUSSION

To better comprehend RSDs and their corresponding ABA signals, this paper (1) models and simulates three common RSDs (rail corrugation, spalling, and squat) with three severity levels (light, moderate, and severe) using explicit dynamic finite element method; (2) processes and analyses simulated RSD-driven ABA signals; and (3) ascertains relationships between RSDs and their corresponding ABA signals.

Results from different signal processing algorithms involving STFT, CWT, EMD, and PSD reveal differences between RSDs, in terms of their temporal and spectral characteristics. Rail corrugation occupies the highest frequency band and has the longest duration, followed by

spalling and squat. Spalling has the lowest signal power magnitude, whereas squat has the highest signal power magnitude. Besides that, the severity of RSDs is proportional to the power magnitude; light severity of RSDs yields low power magnitude, while high severity yields high power magnitude. Processing and analysis of real RSD-driven ABA signals would be necessary to support this claim.

Nonetheless, these findings demonstrate the likelihood of automatically detecting and classifying different types and different severity levels of RSDs from ABA signals, which can increase the efficiency and effectiveness of rail condition monitoring and diagnosis.

ACKNOWLEDGMENT

This research is supported by Land Transport Innovation Fund, Singapore.

REFERENCES

- [1] NSW Transport RailCorp, TMC 226: Rail Defects Handbook. NSW Transport RailCorp, 2012.
- [2] A. K. Ng, Z. B. Alias, J. F. Chassin, and J. H. Yebra, "Managing Rail Corrugation through Modelling, Simulation, and Instrumentation Technologies," Proc. International Conference on IEEE Intelligent Rail Transportation, 2016, pp. 307-314, doi: 10.1109/ICIRT.2016.7588748.
- [3] A. K. Ng, L. Martua, J. H. Yebra, and G. Sun, "Detection and Diagnosis of Rail Surface Defects Using Signal and Image Processing Techniques," Proc. 1st World Congress on Condition Monitoring, 2017, pp. 982-993.
- [4] P. Salvador, V. Naranjo, R. Insa, and P. Teixeira, "Axlebox Accelerations: Their Acquisition and Time-Frequency Characterisation for Railway Track Monitoring Purposes," Measurement, vol. 82, 2016, pp. 301-312.
- [5] M. Molodova, Z. Li, A. Nunez, and R. Dollevoet, "Validation of a Finite Element Model for Axle Box Acceleration at Squats in the High Frequency Range," Computers & Structures, vol. 141, 2014, pp. 84-93.
- [6] Z. Yang, X. Deng, and Z. Li, "Numerical Modeling of Dynamic Frictional Rolling Contact with an Explicit Finite Element Method," Tribology International, vol. 129, 2019, pp. 214-231.
- [7] A. K. Ng, L. Martua, J. H. Yebra, and G. Sun, "Prediction of Rail Corrugation Growth and Rail Wear Rate using Three-Dimensional Finite Element Analysis," Proc. 8th International Conference on Railway Engineering, 2018, pp. 1-6, doi: 10.1049/cp.2018.0055.
- [8] L. Martua, A. K. Ng, and G. Sun, "Prediction of Rail Rolling Contact Fatigue Crack Initiation Life via Three-Dimensional Finite Element Analysis," Proc. International Conference on Intelligent Rail Transportation, 2018, pp. 1-6, doi: 10.1109/ICIRT.2018.8641633.
- [9] A. K. Ng, L. Martua, and G. Sun, "Influence of Sleeper Distance on Rail Corrugation Growth," Proc. International Conference on Intelligent Rail Transportation, 2018, pp. 1-5, doi: 10.1109/ICIRT.2018.8641668.
- [10] M. Molodova, Z. Li, A. Nunez, and R. Dollevoet, "Automatic Detection of Squats in Railway Infrastructure," IEEE Transactions on Intelligent Transportation Systems, vol. 15, 2014, pp. 1980-1990.
- [11] N. E. Huang Z. Shen, S. R. Long, M. C. Wu, H. H. Shih, et al., "The Empirical Mode Decomposition and the Hilbert Spectrum for Nonlinear and Non-Stationary Time Series Analysis," Proceedings of the Royal Society A: Mathematical, Physical and Engineering Sciences, vol. 454, 1998, pp. 903-995.
- [12] S. Singh, U. G. Köpke, C. Q. Howard, and D. Petersen, "Analyses of Contact Forces and Vibration Response for a Defective Rolling Element Bearing using an Explicit Dynamics Finite Element Model," Journal of Sound and Vibration, vol. 333, 2014, pp. 5356-5377.